Available online at www.sciencedirect.com
ScienceDirect
Biochimica et Biophysica Acta 1778 (2008) 880–889
Biochimica et Biophysica Acta BBA
www.elsevier.com/locate/bbamem

Detection of lipid phase coexistence and lipid interactions in sphingomyelin/cholesterol membranes by ATR-FTIR spectroscopy

Zoran Arsov [a,b,*], Luca Quaroni [c]

[a] TASC INFM-CNR, Strada Statale 14- km 163.5, 34012 Basovizza, Trieste, Italy
[b] Sincrotrone Trieste, Strada Statale 14- km 163.5, 34012 Basovizza, Trieste, Italy
[c] Canadian Light Source, 101 Perimeter Rd, Saskatoon (SK), Canada S7N 0X4

Received 26 June 2007; received in revised form 2 November 2007; accepted 17 December 2007
Available online 23 December 2007

Abstract

The phase behavior of binary mixtures of egg sphingomyelin and cholesterol has been inspected by attenuated total reflection Fourier transform infrared (ATR-FTIR) spectroscopy in the amide I′ band reion of the spectrum. Because cholesterol does not have any major absorption bands in this region, effects seen in the spectra of mixtures of sphingomyelin and cholesterol can be attributed to the change in the lipid phase and to the interaction with cholesterol. It is shown that the temperature dependence of the overall bandwidth of the amide I′ band displays a phase-specific behavior. In addition, it is observed that the amide I′ band for a sample exhibiting phase coexistence can be described by a linear combination of the spectra of the individual lipid phases. Description of changes in the amide I′ band shape and by that the study of possible hydrogen bonding interactions of sphingomyelin with cholesterol was assisted by the use of curve fitting. It turns out that the presence of hydrogen bonding between hydroxyl group of cholesterol and carbonyl group of sphingomyelin is obscured by the complexity of different possible hydrogen bonding and coupling between the N–H (N–D) and the C=O group vibrations.

Keywords: Lipid phase coexistence; Cholesterol; ATR-FTIR spectroscopy; Amide I band; Hydrogen bonding

1. Introduction

Model membranes composed of different lipid constituents exhibit lateral phase separation at appropriate temperature and composition [1,2]. Valuable model systems are binary lipid mixtures of phospholipids and cholesterol. In such mixtures, the so called liquid-ordered (cholesterol-rich) phase can exist alone or can coexist with other phases such as gel phase or liquid-disordered phase for appropriate composition and temperature [3]. The question of the nature of interactions that lead to the stabilization of cholesterol-rich phases remains unanswered. It is thought that the largest contribution to cholesterol-phospholipid interactions is from van der Waals forces and hydrophobic forces [4]. On the other hand, it was suggested that the interactions with cholesterol can be strengthened by hydrogen bonding of the cholesterol hydroxyl group to the polar head group and interfacial regions in the phospholipids [5]. In the case of sphingomyelin (SM) species the existence of hydrogen bonding seems particularly plausible since they possess several hydrogen bond-accepting and -donating groups at the polar/non-polar interface [6,7].

Also biological membranes have heterogeneous structures exhibiting coexistence of different lateral lipid domains, among them cholesterol-rich domains, in which lipid molecules have different physical properties [8–10]. There are also some indications of the existence of domains called lipid rafts, with properties similar to the liquid-ordered phase of simple lipid

* Corresponding author. Current address: Laboratory of Biophysics, "Jožef Stefan" Institute, Jamova 39, 1000 Ljubljana, Slovenia. Tel.: +386 1 477 36 48; fax: +386 1 477 31 91.
E-mail address: zoran.arsov@ijs.si (Z. Arsov).

0005-2736/$ - see front matter © 2007 Elsevier B.V. All rights reserved.
doi:10.1016/j.bbamem.2007.12.012

mixtures [11], although lately their existence, as originally conceived, was questioned [12,13]. Usual model systems for lipid rafts are tertiary mixtures of phosphatidylcholines, sphingomyelins and cholesterol. In this respect the study of possible effects of hydrogen bonding in the mixtures of SM and cholesterol is also important.

Infrared (IR) spectroscopy has a number of advantages for the study of lipid membranes. It provides structural and dynamic information from all spectral regions of lipid molecules simultaneously and it does not require spectroscopic probes. Since structural and motional properties of lipids vary between different lipid phases and because the spatial and time scales are appropriate it is expected that IR spectra will be able to reflect phase coexistence [14]. A possible method to use is attenuated total reflection Fourier transform infrared (ATR-FTIR) spectroscopy. The penetration depth of infrared light in the sample is of the order of magnitude of a few hundred nanometers. Consequently, the studies can be performed in the presence of a bulk aqueous phase, while avoiding saturation of the spectrum in the spectral regions where water absorbs [15,16].

The absorption of the amide I band is a potentially interesting region of the IR spectrum of SM for studying properties of different lipid phases. The transition arises mostly from the stretching of the carbonyl group C=O, with minor contributions from the in-plane bending of the C–N–H angle and stretching of the C–N bond [17]. The band is strong and occurs in a region where cholesterol itself does not have any major absorption bands. As a consequence, any effects seen in the spectra of mixtures of SM and cholesterol in this region can be attributed to the change in lipid phase and to the interaction of SM with cholesterol. In addition, the amide II band, which is mainly due to the in-plane bending of the C–N–H angle and stretching of the C–N bond [15,17], can also offer some information on the level and degree of hydrogen bonding to the N–H group.

The amide I band in sphingomyelins is much less studied than the carbonyl band in phosphatidylcholines. The latter is conformationally sensitive, reflects the level of hydration at the membrane interface and is influenced by hydrogen bonding [18]. The present work examines whether similar behavior applies also to the amide I band in sphingomyelins, with a special emphasis on evaluating the importance of hydrogen bonding in the interactions with cholesterol. To our knowledge only one attempt was made to apply infrared spectroscopy to study the effect of cholesterol on the amide I band in mixtures of SM and cholesterol [19]. In this work the authors concluded that hydrogen bonding was present between egg sphingomyelin and cholesterol, based on the downshift of the amide I′[1] band. Our results show that this conclusion is not univocal because of the complexity of the hydrogen bonding network present in this system. Beside the higher number of hydrogen bond-accepting and -donating groups in SM molecules this complexity is also a consequence of possible intermolecular hydrogen bonding interactions among SM molecules themselves [5,20–22].

[1] The amide mode is referred to as amide I′ when measured in D_2O.

The aim of our studies was to use ATR-FTIR spectroscopy and curve fitting to study temperature and composition dependence of the shape of the amide I′ band in different lipid phases of egg sphingomyelin and cholesterol (ESM/Chol) mixtures. The effect of cholesterol was investigated for samples prepared in excess deuterated water as well as for dried samples. We check how the amide I′ band shape changes when SM undergoes the transition from the gel phase to the liquid-disordered phase. Next, we investigate whether phase coexistence can be detected from the shape of the amide I′ band for samples with appropriate amount of cholesterol. Lastly, we explore whether the change in the amide I′ band shape with the addition of cholesterol offers some insight in the nature of intermolecular interactions in the studied system.

2. Materials and methods

2.1. Preparation of liposomes

Egg chicken yolk sphingomyelin (ESM) was obtained from Avanti Polar Lipids (Birmingham, AL, USA). The utilized ESM is highly enriched in long-chain saturated fatty acids, particularly in palmitoyl (84%). Cholesterol and deuterated water (D_2O; 99.9% purity) were obtained from Sigma-Aldrich (St. Louis, MO, USA).

Liposomes were prepared from mixtures of ESM/Chol with varying relative compositions. 20 mg of an appropriate mixture of dry lipids were dissolved in 0.7 ml of chloroform and 0.35 ml of methanol and put in a round-bottom glass flask. The organic solvents were first removed on a rotary evaporator followed by extended drying using a rotary vacuum pump, so as to form a thin lipid film. 1 ml of distilled water was added to the flask. The suspension was in turn hand-shaken and briefly sonicated in a bath sonicator to remove residual lipids from the wall of the glass flask. Next, the suspension was left to hydrate in water for approximately 1 h. The last two steps were done at a temperature around 10 °C above the corresponding temperature of the main phase transition.

2.2. ATR-FTIR spectroscopy

ATR-FTIR spectra were recorded on a Bruker IFS 66v/S infrared spectrometer equipped with a liquid nitrogen cooled mercury–cadmium telluride detector and fitted with a Horizon ATR unit (Harrick Scientific, Pleasantville, NY, USA). The internal reflection element (IRE) was a trapezoidal germanium ATR plate (50×10×2 mm) with an incidence angle of 45° yielding 25 internal reflections (New Era Enterprises, Vineland, NJ, USA). 16 scans were averaged for each spectrum. Spectra were recorded at a nominal resolution of 2 cm^{-1}. The spectrometer and the ATR unit were continuously purged with dry nitrogen gas.

A special holder for the IRE was designed. It was placed in contact with an aluminum block and the temperature was controlled by a circulating water bath connected to the sample mount. The temperature was monitored by a thermocouple placed on the IRE.

2.3. Preparation of sample on internal reflection element

The germanium IRE was cleaned just before use sequentially with distilled water and ethanol. After that, 200 μl of liposome suspension (at a concentration of 20 mg/ml) were added onto the IRE and spread over the whole area. Thin lipid stacks were obtained by evaporating water. The dried samples were not anhydrous. Dried lipid stacks were rehydrated by the addition of 300 μl of pure deuterated water (D_2O) and incubated for some time a few degrees Celsius above the temperature of the main phase transition to allow a complete hydrogen–deuterium exchange as judged from the complete disappearance of the amide II band. For experiments where the amide I′ band was inspected in dried samples, the deposited lipids hydrated with D_2O were dried again. Experiments were carried out in duplicates and new liposomes were prepared each time.

2.4. Analysis of IR spectra

Analysis of ATR-FTIR spectra was done using the OPUS software package, Version 5.5 (Bruker Optics, Ettlingen, Germany).

When the amide I′ band was examined, spectra of samples prepared in D_2O were cut to a frequency range between 1740 and 1520 cm^{-1}. This spectral interval was chosen because the point 1740 cm^{-1} lies in the region well before the absorption band by the amide group, while the point 1520 cm^{-1} lies in the region after the absorption band by the amide group and before the absorption band due to the choline methyl bending modes and the methylene scissoring modes. Then, spectra were baseline corrected with a straight line. Peak positions were determined as points with the maximum amplitude in the amide I′ absorption band. The overall half-bandwidth of the amide I′ band was determined as the width of the band at half the maximum amplitude.

The Fourier self-deconvolution (FSD) and second derivative curves were used to highlight the components of different spectral regions and to determine the approximate values of the peak positions of the components. Bands were deconvolved using a Lorentzian lineshape and a Blackman–Harris apodization function. Bandwidth and noise reduction parameters as defined by OPUS were set so that band components were resolved without causing significant distortions of the deconvolved curves.

Based on the curves obtained by FSD and derivation, three components (one minor and two major) were identified in the amide I′ band. The minor component around 1672 cm^{-1} is denoted as a high-frequency minor (HFm) component. The two major components at approximately 1645 cm^{-1} and 1625 cm^{-1} are denoted as a high-frequency major (HFM) component and a low-frequency major (LFM) component, respectively. However, curve fitting with three components shows poor agreement with the experimental curve on the low-frequency side of the amide I′ band. Subsequently, an additional component at 1590 cm^{-1}, denoted as a low-frequency minor (LFm) component, was used. This component might represent carbonyl groups involved in more than one hydrogen bond. Consequently, the amide I′ band was fitted with four components using the Levenberg–Marquardt method. The peak positions of the resolved components were fixed to the values obtained by FSD and second derivatives. It has to be pointed out that the HFM component for pure ESM was only seen as a shoulder. For the HFM component in pure ESM samples and for the LFm component the peak positions were estimated by fitting. The peak position (width) of the HFm component was fixed at 1673 cm^{-1} (14 cm^{-1}) for ESM and at 1672 cm^{-1} (14 cm^{-1}) for ESM/Chol 0.4. The assignment of this peak is not clear. The peak position (width) of the LFm component was fixed at 1590 cm^{-1} (40 cm^{-1}) for all samples. The percent of contribution of Lorentzian shape to the overall Lorentzian–Gaussian lineshape for the components from high to low frequency were fixed at 100%, 0%, 10%, and 0% of Lorentzian contribution, respectively. The reason for such a choice for the last three values was that the best fits, as judged by the residual root-mean-square, were usually achieved with such values. The value of the Lorentzian contribution for the HFm component was fixed at 100%, but due to a relatively low contribution of this component to the overall fit, this value did not affect significantly the fitting results. The remaining parameters, i.e. the intensities and the widths of the two major components, were allowed to vary. Fitting always gave unique solutions irrespective of the starting values of parameters. The variability of the fitting parameters was estimated by changing the value of the peak positions of the two major components and then repeating the fitting; the value was changed in the interval determined by the uncertainty of the peak position obtained by FSD and second derivatives for the well resolved components, whereas in the case of the HFM component for pure ESM the value was changed in the interval that caused a comparable deviation from the minimum value of residual root-mean-square. After the fitting procedure, the relative contribution of a particular component was calculated from the integrated areas of individual components.

The procedure of linear superposition of spectra was set in Mathematica, Version 5.0 (Wolfram Research, Champaign, IL, USA). The weights of spectra for ESM and ESM/Chol 0.4 samples were automatically adjusted so that the root-mean-square of the deviations between the experimental spectrum for ESM/Chol 0.2 samples and the curve obtained by linear superposition reached a minimum. Before superposition, experimental spectra were normalized to the same area.

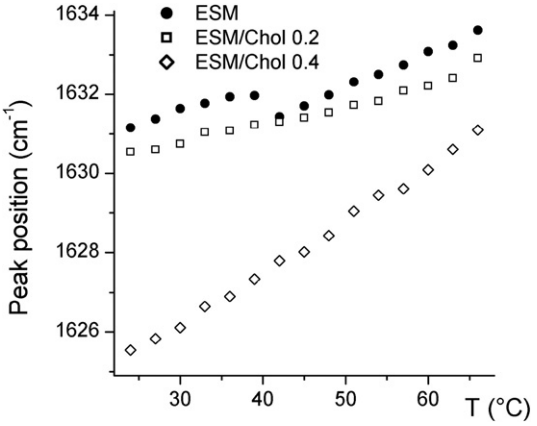

Fig. 2. Temperature dependence of amide I′ band peak position for hydrated ESM/Chol samples with different mole fractions of cholesterol. Each point represents an average value from two different experiments. Estimate of the uncertainty in the peak position is ±0.2 cm^{-1}.

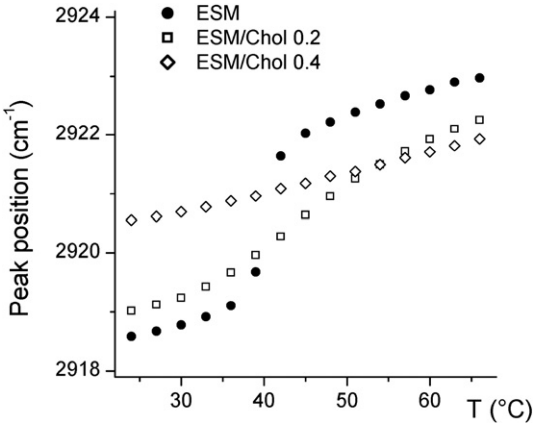

Fig. 1. Temperature dependence of methylene antisymmetric stretching band peak position for hydrated ESM/Chol samples with different mole fractions of cholesterol. Each point represents an average value from two different experiments. Estimate of the uncertainty in the peak position is ±0.1 cm^{-1}.

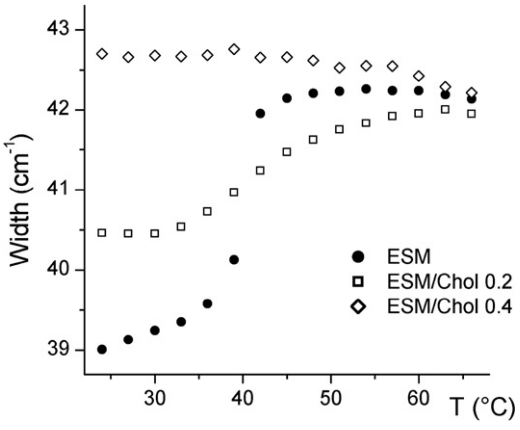

Fig. 3. Temperature dependence of half-bandwidth of amide I′ band for hydrated ESM/Chol samples with different mole fractions of cholesterol. Each point represents an average value from two different experiments. Estimate of the uncertainty in the half-bandwidth is ±0.2 cm^{-1}.

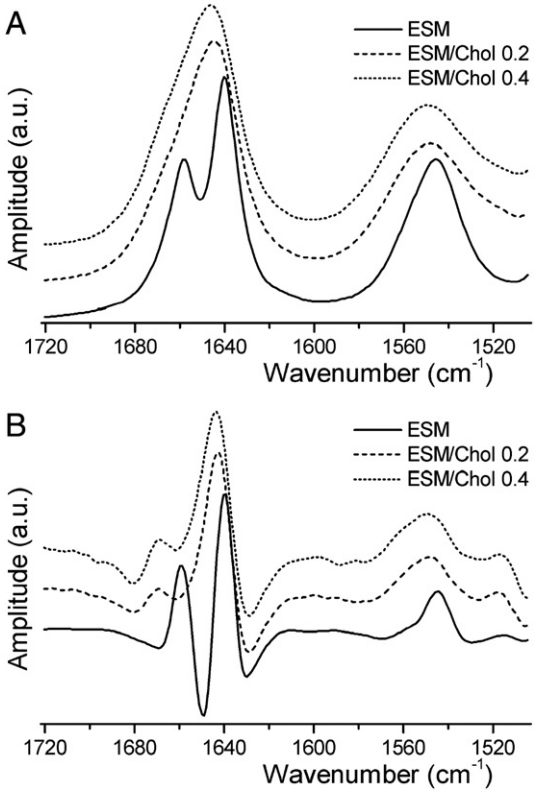

Fig. 4. Dependence of the amide I/amide II band region for dried ESM/Chol samples on mole fraction of cholesterol: (A) ATR-FTIR spectra, (B) curves obtained by taking the negative value of the second derivative. The amplitudes of the spectra (curves) were set to an arbitrary value. Spectra from one experiment are shown.

ATR-FTIR spectra from different experiments for the same samples showed similar behavior with temperature and cholesterol mole fraction. Accordingly, the results of the peak analysis and parameters of the curve fitting procedure are shown as averages. Where spectra are presented, spectra from one experiment are shown.

3. Results

The temperature dependence of the methylene antisymmetric stretching peak position, which reflects lipid conformation, is shown in Fig. 1. Results show that a large shift in peak frequency occurs near the temperature of the main phase transition, T_m. This is around 41 °C for palmitoyl SM [23] and around 39 °C for egg SM [24]. For samples with 0.2 mole fraction of cholesterol

Table 1
Peak positions of the amide I (I′) doublet in dried ESM samples and corresponding differences Δ

	Peak position (diff.) of Low-Frequency Peak (cm^{-1})	Peak position (diff.) of High-Frequency Peak (cm^{-1})	Δ (cm^{-1})
amide I	1640	1658	18
amide I′	1628	1650	22
Δ(I-I′)	12	8	

Table 2
Dependence of peak positions of the amide II mode on cholesterol in dried ESM samples

	Peak position (cm^{-1})
ESM	1545.8 (0.3)
ESM/Chol 0.2	1548.5 (0.5)
ESM/Chol 0.4	1549.5 (0.3)

The values in parentheses are estimates of uncertainty.

(ESM/Chol 0.2), the slope becomes steeper above T_m and then less steep again for higher temperatures (Fig. 1). In contrast, ESM/Chol 0.4 samples show a linear increase in frequency.

The temperature dependence of the amide I′ band position for samples with different mole fractions of cholesterol is shown in Fig. 2. For pure ESM it can be seen that a small shift of the peak position to lower frequencies occurs near the temperature of the main phase transition T_m, but else the frequency shows a steady increase with temperature either below T_m or above T_m. For ESM/Chol 0.2 samples no specific feature is seen at T_m and the peak position shows a steady increase with temperature over the whole temperature interval. Similarly, ESM/Chol 0.4 samples also show a linear increase of the peak position with temperature, although more steep than in the case of ESM/Chol 0.2 samples.

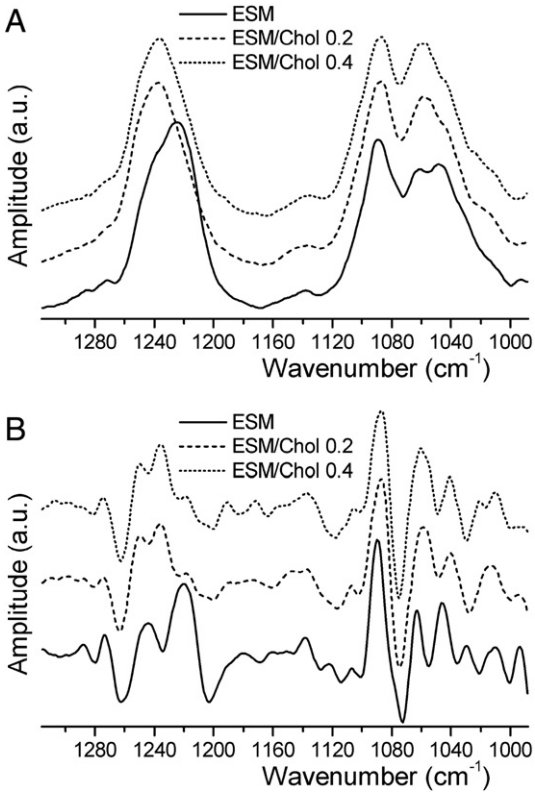

Fig. 5. Dependence of the phosphate group bands region for dried ESM/Chol samples on mole fraction of cholesterol: (A) ATR-FTIR spectra, (B) curves obtained by taking the negative value of the second derivative. The amplitudes of the spectra (curves) were set to an arbitrary value. Spectra from one experiment are shown.

It was observed that the shape of the amide I′ band for ESM sample shows significant broadening with temperature. This pattern becomes evident if we report the change of the overall half-bandwidth of the amide I′ band with temperature (Fig. 3). Moreover, the main phase transition is detected through the sharp increase of the half-bandwidth at T_m for pure ESM (Fig. 3). In addition, the influence of cholesterol could also be appreciated. For ESM/Chol 0.2 the slope changes its steepness above T_m, while for ESM/Chol 0.4 the half-bandwidth stays almost constant (Fig. 3). It has to be emphasized that the amide I′ band is a composite band, as shown below, and consequently the half-bandwidth can only be used as an empirical parameter. Its value depends on the half-bandwidth, positions and intensities of particular components comprising the band. Nevertheless, the overall bandwidth is relevant, because it conveys valuable information about molecular properties of the sample without the need of further spectra manipulation.

In Fig. 4A the amide I/amide II region of the ATR-FTIR spectra of dried samples is shown. It can be seen that the amide I doublet, around 1650 cm^{-1} for pure ESM, is smeared by the presence of cholesterol for Chol 0.2 samples. The peak positions for the amide I and the amide I′ doublet in dried ESM samples and their differences are summarized in Table 1. The corresponding second derivative curves in Fig. 4B show that also the amide II band around 1550 cm^{-1} is influenced by the presence of cholesterol (Fig. 4). The peak position as well as the width increase with cholesterol concentration (Table 2, Fig. 4). The same effects on the amide II band are observed also for samples prepared in excess H_2O (data not shown).

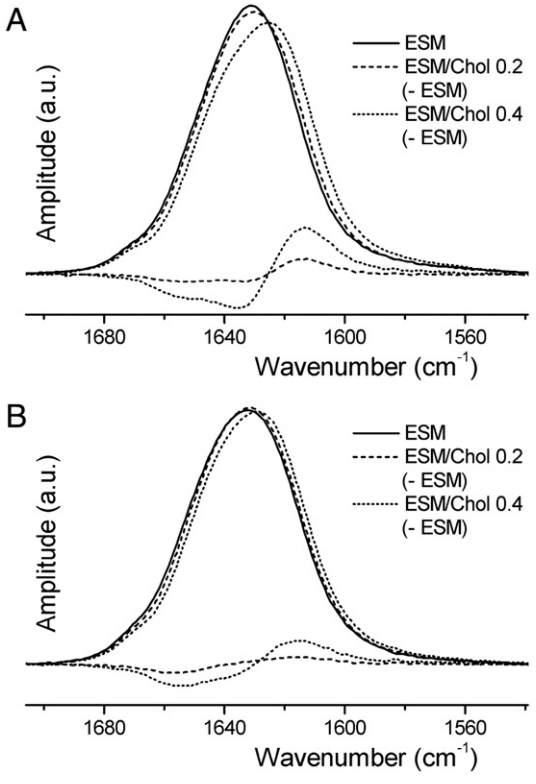

Fig. 6. Dependence of the amide I′ band shape on mole fraction of cholesterol and corresponding subtraction curves for hydrated ESM/Chol samples: (A) at temperature 24 °C (below the temperature of the main phase transition T_m), (B) at temperature 54 °C (above T_m). Absorption bands were normalized to the same area. The subtraction curves (shown at the bottom) were obtained by subtraction of the amide I′ band of pure sample from the amide I′ band of cholesterol containing samples. Spectra from one experiment are shown.

Table 3
Peak positions of the two major amide I′ band components obtained from FSD and second derivatives

	Peak position of LFM component (cm^{-1})		Peak position of HFM component (cm^{-1})	
	ESM	ESM/Chol 0.4	ESM	ESM/Chol 0.4
T=24 °C	1629.0 (0.3)	1621.0 (0.3)	1648, shoulder	1641.9 (0.3)
T=36 °C	1629.5 (0.3)	1622.0 (0.3)	1649, shoulder	1642.5 (0.4)
T=42 °C	1625.8 (0.4)	1622.5 (0.3)	1644, shoulder	1642.8 (0.4)
T=54 °C	1626.5 (0.4)	1623.7 (0.3)	1645, shoulder	1643.5 (0.5)

The values in parentheses are estimates of uncertainty.

The effect of cholesterol in dried samples can also be appreciated in the spectral region of phosphate group vibrations (Fig. 5). The shape of the band at around 1230 cm^{-1} associated with the antisymmetric phosphate group stretching shows significant change with cholesterol. On the contrary, there is only a slight effect of cholesterol on the symmetric phosphate group stretching band at around 1090 cm^{-1} (Fig. 5). A very clear effect of cholesterol was seen also for the diester phosphate stretching band at around 1060 cm^{-1}. For pure ESM this band is split, while the splitting is smeared in the case of cholesterol containing samples (Fig. 5A). Cholesterol also has an absorption band in this region, around 1055 cm^{-1}, which is assigned to the stretch of the cholesterol C–O group [25]. Nonetheless, subtracting the spectrum of pure cholesterol does not change the above conclusions (data not shown).

Fig. 6 presents overlaid spectra normalized to the same area to highlight differences in the shape of the amide I′ band for samples of ESM with different amounts of cholesterol prepared in excess D_2O. The difference is much more obvious for the temperature below T_m (Fig. 6A). The asymmetry in the shape of the amide I′ band (Fig. 6A) as well the bandwidth (Figs. 6A, 3) increases for samples with cholesterol. In addition, the curve for ESM/Chol 0.4 is strongly downshifted (Figs. 6A, 2). Subtraction curves shown at the bottom of Fig. 6, obtained after subtraction of the amide I′ band of the pure samples from the amide I′ band of the samples containing cholesterol, clearly show the effect of cholesterol.

FSD and second derivative curves were used to check how the addition of cholesterol affects the peak positions of the components making up the amide I′ band. Three components, one minor at higher frequency, denoted as the HFm component, and two major at higher and lower frequency denoted as the HFM and LFM components, respectively, were resolved (see the subsection Analysis of IR spectra in the Materials and methods for details). The results for the two major components for ESM and ESM/Chol 0.4 are summarized in Table 3. For all temperatures the peak positions for

both components significantly decrease with the addition of cholesterol.

We tested how well we can describe the shape of spectra of the ESM/Chol 0.2 samples with superposition of the corresponding spectra for pure ESM and for ESM/Chol 0.4, since ESM/Chol 0.2 samples are expected to display spectral contributions from both coexisting lipid phases. ESM/Chol 0.2 spectra can be nicely described by a superposition of spectra for ESM and ESM/Chol 0.4. The result for T=24 °C is shown in Fig. 7. A similarly good agreement was obtained also for all other temperatures (data not shown). The weight of ESM spectra was around 60−70%, while the weight of ESM/Chol 0.4 spectra was around 30−40%.

The temperature dependence of the shape of the amide I′ band region for ESM and ESM/Chol 0.4 is shown in Fig. 8A and B, respectively. In addition, the corresponding second derivative curves are presented as insets of Fig. 8. The bandwidth for ESM samples increases for temperatures above T_m (Fig. 8A), mainly due to the downshift of the LFM component and the increase of the intensity of the HFM component (see inset of Fig. 8A). In the case of ESM/Chol 0.4 samples, the spectra are very similar to each other except that the whole band gradually moves to higher frequencies (Fig. 8B). As seen from comparison of Fig. 8A and B the larger asymmetry in the shape of the amide I′ band for ESM/Chol 0.4 compared to ESM for temperature below T_m, discernible also in Fig. 6A, is a consequence of a relatively large intensity of the HFM component for ESM/Chol 0.4.

The amide I′ band was fitted with four components (see the subsection Analysis of IR spectra in the Materials and methods for details). The results of the curve fitting for the two major HFM and LFM components are summarized in Table 4. The following parameters are shown for each component: peak position (Peak), intensity (Intens.), width (Width), relative integrated areas (Rel. Integr.). Table 4 lists fitting parameters and differences in peak positions of the two components (Δ(Peak)),

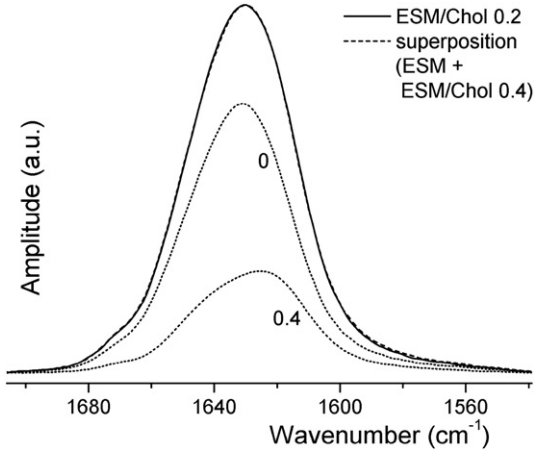

Fig. 7. Comparison of the amide I′ band region of an experimental ATR-FTIR spectrum for hydrated ESM/Chol 0.2 sample at temperature 24 °C and a curve obtained by superposition of corresponding experimental spectra for ESM (curve 0) and ESM/Chol 0.4 (curve 0.4). For the weights used and other details see text.

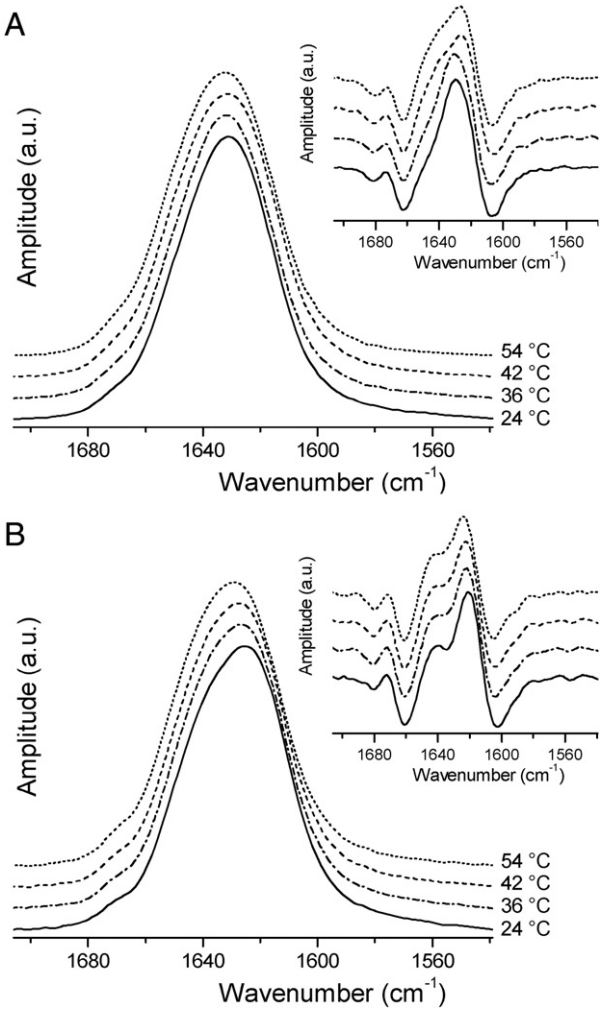

Fig. 8. Temperature dependence of the amide I′ band region for hydrated (A) ESM and (B) ESM/Chol 0.4 samples. Inset shows corresponding curves obtained by taking the negative value of the second derivative. Absorption bands were normalized to the same intensity (amplitude). Spectra from one experiment are shown.

as well as differences in peak positions of the same component for ESM or ESM/Chol 0.4 samples (Δ(ESM–ESM/Ch)). The relative integrated areas of the HFm component at 1673 cm^{-1} (1672 cm^{-1}) were around 0.02 for ESM and around 0.03 for ESM/Chol 0.4. The relative integrated area of the LFm component at 1590 cm^{-1} was on average around 0.05 for ESM and around 0.07 for ESM/Chol 0.4. For both components these values did not change significantly with temperature.

In Fig. 9 the amide I′ band and fit components are shown for temperature below T_m and for temperature above T_m for hydrated ESM (Fig. 9A) and ESM/Chol 0.4 (Fig. 9B) samples. In the case of ESM the most significant change going from the gel phase S to the liquid-disordered phase Ld is an increase in the intensity of the HFM component (Fig. 9A, Table 4). In the case of ESM/Chol 0.4 samples, which are in the liquid-ordered phase Lo for all temperatures, only moderate changes occur (Fig. 9B, Table 4). It is interesting to note that the difference in the peak positions between the HFM

Table 4
Parameters of the amide I′ band curve fitting (for the two major components)

		LFM component				HFM component				
		Peak (cm^{-1})	Intens. (a.u.)	Width (cm^{-1})	Rel. Integr.	Peak (cm^{-1})	Intens. (a.u.)	Width (cm^{-1})	Rel. Integr.	Δ(Peak) (cm^{-1})
T=24 °C	ESM	1629.0 (0.3)	1.04 (0.01)	32.6 (0.5)	0.75 (0.02)	1649.0 (0.6)	0.30 (0.02)	28.0 (1.3)	0.18 (0.01)	20.0 (0.9)
	ESM/ Chol 0.4	1621.0 (0.3)	0.85 (0.02)	28.1 (0.3)	0.53 (0.02)	1641.9 (0.3)	0.60 (0.01)	28.6 (0.9)	0.36 (0.01)	20.9 (0.6)
	Δ(ESM- ESM/Ch)	8.0 (0.6)				7.0 (0.9)				
T=36 °C	ESM	1629.5 (0.3)	1.03 (0.01)	33.1 (0.7)	0.75 (0.02)	1649.4 (0.6)	0.31 (0.02)	28.2 (1.1)	0.18 (0.01)	19.9 (0.9)
	ESM/ Chol 0.4	1622.0 (0.3)	0.83 (0.02)	29.0 (0.6)	0.53 (0.02)	1642.5 (0.4)	0.59 (0.02)	29.2 (0.9)	0.36 (0.01)	20.5 (0.7)
	Δ(ESM–ESM/Ch)	7.5 (0.6)				7.0 (1.0)				
T=42 °C	ESM	1625.8 (0.4)	0.83 (0.02)	31.4 (0.7)	0.58 (0.02)	1645.3 (0.6)	0.54 (0.03)	30.6 (1.2)	0.35 (0.01)	19.5 (1.0)
	ESM/Chol 0.4	1622.5 (0.3)	0.82 (0.02)	29.3 (0.5)	0.53 (0.02)	1642.8 (0.4)	0.59 (0.02)	29.5 (0.9)	0.37 (0.01)	20.3 (0.7)
	Δ(ESM–ESM/Ch)	3.3 (0.7)				2.5 (1.0)				
T=54 °C	ESM	1626.5 (0.4)	0.82 (0.02)	31.9 (0.8)	0.58 (0.02)	1646.1 (0.6)	0.54 (0.03)	31.1 (1.3)	0.36 (0.02)	19.5 (1.0)
	ESM/Chol 0.4	1623.7 (0.3)	0.81 (0.03)	30.3 (0.7)	0.54 (0.02)	1643.5 (0.5)	0.59 (0.03)	30.0 (1.0)	0.37 (0.01)	19.9 (0.8)
	Δ(ESM–ESM/Ch)	2.9 (0.7)				2.5 (1.1)				

The values in parentheses are estimates of uncertainty of a particular parameter.

and LFM components is around 20 cm^{-1} for all samples and temperatures (see Table 4).

4. Discussion

The temperature-composition phase diagram for binary mixtures of palmitoyl SM (PSM) or egg SM (ESM) with cholesterol has a similar shape than the phase diagram for mixtures of phosphatidylcholines and cholesterol (Fig. 10). The most obvious difference is a much higher temperature of disappearance of the coexistence region of the liquid phases, which was already pointed out before for the case of bovine brain sphingomyelin [26]. The phase diagram presented in Fig. 10 was constructed from previous experimental data and from data obtained in the current experiment. Joint presentation of data for PSM and ESM is justified by a high content of palmitoyl chains in ESM (see the Materials and methods for details). Published data were obtained by differential scanning calorimetry [27–29], fluorescence spectroscopy [30], nuclear magnetic resonance spectroscopy [31], and electron paramagnetic resonance spectroscopy [32,33]. Approximate schematic lines representing

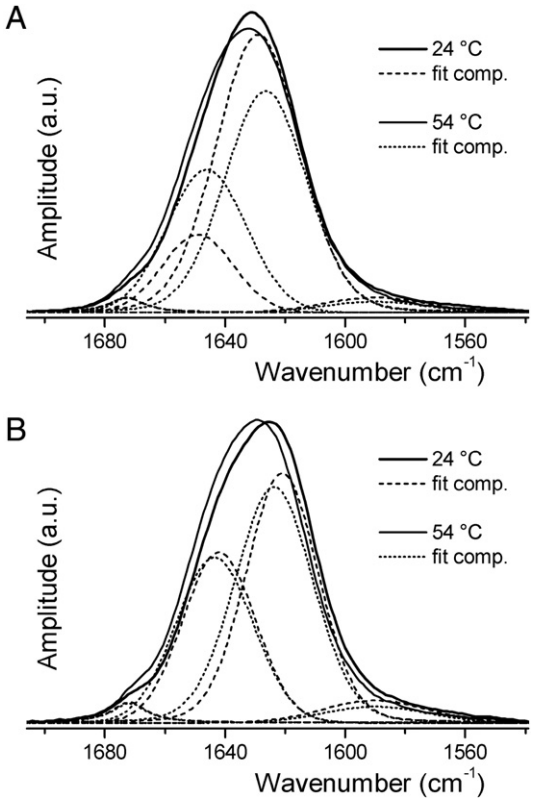

Fig. 9. Comparison of the amide I′ band region of ATR-FTIR spectra for hydrated ESM/Chol samples at temperatures above and below the temperature of the main phase transition T_m: (A) ESM, (B) ESM/Chol 0.4. The thick and the thin solid lines represent experimental spectra normalized to the same area. The corresponding dashed and dotted lines represent our estimates of the underlying components obtained by curve fitting. For fit parameters see Table 4. Spectra from one experiment are shown.

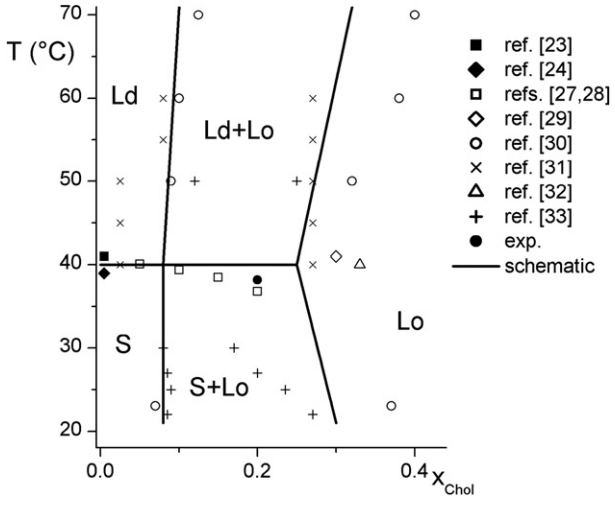

Fig. 10. Schematic temperature-composition phase diagram for binary mixture palmitoyl (egg) SM/Chol. Data points were obtained from literature and from the current experiment (exp.). Lines represent schematic phase boundaries. At the horizontal line (temperature T_m) the main phase transition occurs. Lipid phases and phase coexistence regions are denoted as: gel phase S, liquid-ordered phase Lo, liquid-disordered phase Ld and coexistence regions of the S and Lo phases (S+Lo) and of the Ld and Lo phases (Ld+Lo). Mole fraction of cholesterol is denoted by x_{Chol}.

phase boundaries were drawn with the purpose of highlighting the different phase regions (Fig. 10).

It is expected that infrared spectra will reflect the presence of different lipid phases, phase coexistence regions, and transitions between them. The temperature dependence of the peak position of the methylene antisymmetric stretching mode (Fig. 1) shows a phase-specific behavior, while it reflects both the main phase transition for pure ESM as well as the transition between the two phase coexistence regions for ESM/Chol 0.2. In addition, the peak exhibits a steady shift for ESM/Chol 0.4 (Fig. 1), in agreement with the presence of the single Lo phase for all temperatures (Fig. 10). Similar behavior can also be seen for the temperature dependence of the half-bandwidth of the amide I′ band (Fig. 3), while the amide I′ band peak position seems much less susceptible to phase transitions (Fig. 2). Results presented in Figs. 2 and 3 show that beside other factors the amide I′ band is influenced also by the change in the lipid conformation. The point obtained from our experimental data in Fig. 10 was determined as the temperature at which the curves for ESM/Chol 0.2 samples in Figs. 1 and 3 change their slopes. In addition, the phase coexistence for ESM/Chol 0.2 samples was directly detected from the shape of the amide I′ band, as it could be described as a superposition of the amide I′ band for pure ESM and ESM/Chol 0.4 (Fig. 7).

The effect of the addition of cholesterol on the shape of ATR-FTIR spectra was first studied for dried samples. The amide I band is split into two peaks in dried sphingomyelin samples (Fig. 4) presumably due to intermolecular interactions between neighboring SM molecules [34]. The reported values of the peak positions 1656 cm^{-1} and 1639 cm^{-1} for ESM [34], and 1658 cm^{-1} and 1641 cm^{-1} for bovine brain SM [22] are close to the values obtained in the current experiment (see Table 1). For the amide I′ band we determined values 1650 cm^{-1} and 1628 cm^{-1}, respectively, in accordance with the previously established values for bovine brain SM [35]. The peak at lower frequency of amide I band has been assigned to the population of SM molecules whose carbonyl oxygen is involved in hydrogen bonding. The peak at higher frequency represents the population of nonhydrogen- or weakly hydrogen-bonded ESM molecules. The latter is supported also by data reported for amide I frequency of around 1657 cm^{-1} for ceramides dissolved in chloroform [36].

Intermolecular interactions cause a difference of around 20 cm^{-1} in the frequency of the doublet peaks of the amide I (I′) band (Table 1). This number is close to the values reported for *N*-methylacetamide [37]. In addition, if the N–H group in *N*-methylacetamide is hydrogen-bonded (either to the C=O group or to water), this has a comparable effect on the amide I frequency as a direct hydrogen bond to the C=O group [37,38]. Due to this coupling it is possible that the ESM–ESM intermolecular hydrogen bond involving the oxygen of the hydroxyl group and the hydrogen of the N–H group might also downshift the amide I band frequency.

The addition of cholesterol has a strong effect on the amide I band in dried samples (Fig. 4A). The amide I band is still asymmetric, although the splitting is unresolved (Fig. 4B). The reason for this is probably that beside ESM–ESM intermolecular interactions also interaction with cholesterol is possible, increasing the heterogeneity of the environment surrounding the amide group. Even though our dried samples are not anhydrous, the amount of water molecules in the samples is very low as judged from the shape of the band from approximately 3700 to 3100 cm^{-1} corresponding to the O–H and N–H stretching modes and is not higher in the cholesterol containing samples (data not shown). Therefore, it is reasonable to expect that the observed effect of cholesterol is primarily due to the interaction between ESM and cholesterol and not due to the putative presence of water molecules. Cholesterol has a strong effect also on the amide II band, perturbing both the peak position and the bandwidth (Fig. 4). The increase in the frequency of the amide II band suggests an increased level of hydrogen bonding [17]. Either hydrogen bonds are formed with cholesterol or the pattern of ESM–ESM intermolecular hydrogen bonding is affected.

In addition to the amide region, also the phosphate group region of the spectra was inspected. In accordance with previous studies for dry [22] and hydrated samples [21], the antisymmetric phosphate group stretching band is asymmetric (Fig. 5A) and composed of at least two components (Fig. 5B). The component at lower frequencies is thought to represent a population of phosphate groups involved in inter- or intramolecular interactions [21]. It can be seen that the addition of cholesterol diminishes the component representing interacting molecules. It has to be said here that the studied samples were not anhydrous. Therefore, it is possible that also water molecules that are still present after drying affect the phosphate band shape. This effect might be different, if cholesterol influences the amount of the trapped water. In contrast, the symmetric phosphate group stretching band is much less sensitive to the addition of cholesterol (Fig. 5). Similar results were also obtained from hydration studies [39], indicating that the phosphate symmetric stretching band is less sensitive to hydrogen bonding than the antisymmetric stretching band. Furthermore, the splitting of phosphate diester stretching band was resolved for the first time (Fig. 5A). This splitting might be indicative of intramolecular interaction involving phosphate ester oxygen, whose existence was shown in hydrated samples by molecular dynamics simulation [40–43].

In addition to the dried samples, also the influence of cholesterol on the shape of the amide I′ band for hydrated samples was demonstrated (Fig. 6). Subtraction curves in Fig. 6 confirm that the amide I′ band region of infrared spectrum reflects an interaction between cholesterol and sphingomyelin.

The data obtained by FSD and second derivatives show that the amide I′ band in hydrated samples is composed of two major components (see Fig. 8A, B and Table 3). The LFM component of the amide I′ band is ascribed to the population of molecules forming hydrogen bonds. In addition to hydrogen bonds due to intermolecular ESM–ESM interaction, the possibility of hydrogen bonding to water molecules has to be taken into account in hydrated samples. The presence of only one low-frequency major component indicates that the effect of hydrogen bonding to water molecules is comparable to the effect of ESM–ESM intermolecular hydrogen bond. This is in accordance with the findings for *N*-methylacetamide, where in

both cases the shift was comparable and was around 20 cm^{-1} [37,38]. The case of ESM/Chol 0.4 samples is more complex, because hydrogen bonding to cholesterol is also possible.

It can be observed from the second derivative curves (see inset of Fig. 8A) that the peak position of the LFM component downshifts at the main phase transition. The downshift is about 4 cm^{-1} (Table 3), close to the previously determined value [19]. In the work by Veiga et al. [19] the asymmetry of amide I′ band was not taken into account and no observation was made of the change of the peak position of the HFM component with temperature. We report a downshift of the HFM component of around 4 cm^{-1} at T_m (Table 4). Since the downshifts of both major components of the amide I′ band are comparable, the difference in their peak positions remains the same, i.e. around 20 cm^{-1}, below and above T_m (Table 4). The origin of these downshifts are either conformational effects or changed proportions of different types of hydrogen bonds, e.g. changed ratio between the number of ESM–ESM intermolecular hydrogen bonds and the number of hydrogen bonds with (deuterated) water.

This behavior is markedly different than in the case of the carbonyl band in saturated phosphatidylcholines, where the peak positions of the components comprising the carbonyl band only slightly increase for temperatures above T_m [16].

It can be seen from the second derivative curves (inset of Fig. 8A) and from the curve fitting parameters (Table 4) that the increase in the intensity of the HFM component is the most pronounced change with temperature for pure ESM. A similar effect was already seen for gangliosides, where it was suggested that this could be an indication of lower hydration level in the Ld phase [44]. In addition, D_2O quadrupolar splittings indicate that the sphingomyelin lipid–water interface is less polar above the main phase transition temperature [45]. On the other hand, another possible explanation would be a decrease in the number of ESM–ESM intermolecular hydrogen bonds. In principle it would be possible to deduce the variation in the ratio between the number of hydrogen bonds with water and the number of ESM–ESM intermolecular hydrogen bonds when going through the main phase transition from molecular dynamics simulation studies. Unfortunately, such studies are only reported for temperature values above T_m [43,46].

The observed behavior of the amide I′ band in ESM is just the opposite of the one found for carbonyl band in phosphatidylcholines, where the main phase transition is accompanied by the increase of the intensity of the low-frequency component of the carbonyl band reflecting the increased level of hydration [16,34].

Curve fitting analysis was used to quantify differences between pure ESM and ESM/Chol 0.4 samples (Fig. 9). In accordance with previous results [19], the peak position of the LFM component of the amide I′ band for ESM/Chol 0.4 is significantly decreased both below and above T_m compared to pure ESM. This decrease was attributed to the formation of hydrogen bonds between cholesterol and sphingomyelin [19]. In contrast, our work shows that both components of the amide I′ band are downshifted by a similar amount. Therefore, it is not possible to interpret the observed shift of the LFM component as simply due to hydrogen-bond formation involving cholesterol and the C=O group. For example, a conformational change of the SM molecules induced by cholesterol could be responsible for this downshift.

In addition, curve fitting also shows that a large decrease in the width of the LFM component by about 4 cm^{-1} for ESM/Chol 0.4 as compared to ESM is present below T_m (Table 4), even though the number of possible different hydrogen bonds increases. The reason for this might be the disruption of ESM–ESM intermolecular hydrogen bonds by cholesterol as suggested by molecular dynamics simulations [42,46]. This possibility has been proposed already before for mixtures of cerebrosides and cholesterol [47].

In conclusion, lipid phase properties in ESM/Chol samples as well as the interaction between cholesterol and ESM were studied by the use of ATR-FTIR spectroscopy over a temperature range. Spectroscopic data confirmed the structure of the phase diagram for ESM/Chol mixtures. It was also shown that addition of cholesterol to ESM induces a series of perturbations in the vibrational properties on ESM. We show that, in the case of dried mixtures, hydrogen bonding between ESM and cholesterol appears to be important in defining intermolecular interactions. In the presence of bulk water, addition of cholesterol also perturbs ESM. However, in contrast to the dried systems, the complexity of the hydrogen bonding network prevents us from isolating one specific interaction between cholesterol and ESM. Our work clearly shows that intermolecular interactions play a role in defining the molecular properties of ESM/Chol mixtures. By extension, it is possible that similar interactions could be involved in defining the thermodynamic stability and molecular properties of cholesterol-rich lipid domains and related mixed lipid systems.

Acknowledgements

This work was carried out with the financial support of the Sincrotrone Trieste. Z.A. acknowledges the financial support from the state budget by the Slovenian Research Agency (programme No. P1-0060, project No. Z1-9502). The authors thank Dr. J. Grdadolnik for helpful discussions, Prof. G. Scoles for supporting the purchase of the ATR unit, and Coherentia INFM-CNR for providing access to the interferometer. The authors are also thankful for personal communications with Dr. M. E. Rerek, Prof. R. Mendelsohn and Prof. M. Pasenkiewicz-Gierula. Z.A. was supported by a postdoctoral fellowship through the INTERREG IIIA Italy–Slovenia European programme of cross-border cooperation.

References

[1] E.J. Shimshick, H.M. McConnell, Lateral phase separation in phospholipid membranes, Biochemistry 12 (1973) 2351–2360.
[2] Z. Arsov, J. Štrancar, Determination of partition coefficient of spin probe between different lipid membrane phases, J. Chem. Inf. Model. 45 (2005) 1662–1671.
[3] J.H. Ipsen, G. Karlström, O.G. Mouritsen, H. Wennerström, M.J. Zuckermann, Phase equilibria in the phosphatidylcholine-cholesterol system, Biochim. Biophys. Acta 905 (1987) 162–172.

[4] T.P.W. McMullen, R.N. McElhaney, Physical studies of cholesterol-phospholipid interactions, Curr. Opin. Colloid Interface Sci. 1 (1996) 83–90.
[5] J.M. Boggs, Lipid intermolecular hydrogen bonding: influence on structural organization and membrane function, Biochim. Biophys. Acta 906 (1987) 353–404.
[6] H. Ohvo-Rekila, B. Ramstedt, P. Leppimaki, J.P. Slotte, Cholesterol interactions with phospholipids in membranes, Prog. Lipid Res. 41 (2002) 66–97.
[7] B. Ramstedt, J.P. Slotte, Sphingolipids and the formation of sterol-enriched ordered membrane domains, Biochim. Biophys. Acta 1758 (2006) 1945–1956.
[8] R. Welti, M. Glaser, Lipid domains in model and biological membranes, Chem. Phys. Lipids 73 (1994) 121–137.
[9] F.R. Maxfield, Plasma membrane microdomains, Curr. Opin. Cell Biol. 14 (2002) 483–487.
[10] Z. Arsov, M. Schara, J. Štrancar, Quantifying the lateral lipid domain properties in erythrocyte ghost membranes using EPR-spectra decomposition, J. Magn. Reson. 157 (2002) 52–60.
[11] E. London, How principles of domain formation in model membranes may explain ambiguities concerning lipid raft formation in cells, Biochim. Biophys. Acta 1746 (2005) 203–220.
[12] M. Edidin, The state of lipid rafts: from model membranes to cells, Annu. Rev. Biophys. Biomol. Struct. 32 (2003) 257–283.
[13] T.P.W. McMullen, R.N.A.H. Lewis, R.N. McElhaney, Cholesterol-phospholipid interactions, the liquid-ordered phase and lipid rafts in model and biological membranes, Curr. Opin. Colloid Interface Sci. 8 (2004) 459–468.
[14] J. Štrancar, Z. Arsov, Application of spin labeling EPR and ATR-FTIR spectroscopies to the study of membrane heterogeneity, in: A. Leitmannova Liu (Ed.), Advances in Planar Lipid Bilayers and Liposomes, vol. 6, Elsevier, Amsterdam, 2008, pp. 139–163.
[15] L.K. Tamm, S.A. Tatulian, Infrared spectroscopy of proteins and peptides in lipid bilayers, Q. Rev. Biophys. 30 (1997) 365–429.
[16] Z. Arsov, L. Quaroni, Direct interaction between cholesterol and phosphatidylcholines in hydrated membranes revealed by ATR-FTIR spectroscopy, Chem. Phys. Lipids 150 (2007) 35–48.
[17] G.C. Pimentel, A.L. McClellan, The Hydrogen Bond, W. H. Freeman, San Francisco, 1960.
[18] R.N.A.H. Lewis, R.N. McElhaney, W. Pohle, H.H. Mantsch, Components of the carbonyl stretching band in the infrared spectra of hydrated 1,2-diacylglycerolipid bilayers: a reevaluation, Biophys. J. 67 (1994) 2367–2375.
[19] M.P. Veiga, J.L.R. Arrondo, F.M. Goni, A. Alonso, D. Marsh, Interaction of cholesterol with sphingomyelin in mixed membranes containing phosphatidylcholine, studied by spin-label ESR and IR spectroscopies. A possible stabilization of gel-phase sphingolipid domains by cholesterol, Biochemistry 40 (2001) 2614–2622.
[20] I. Pascher, Molecular arrangements in sphingolipids. Conformation and hydrogen bonding of ceramide and their implication on membrane stability and permeability, Biochim. Biophys. Acta 455 (1976) 433–451.
[21] J. Villalain, A. Ortiz, J.C. Gomez-Fernandez, Molecular interactions between sphingomyelin and phosphatidylcholine in phospholipids vesicles, Biochim. Biophys. Acta 941 (1988) 55–62.
[22] O.P. Lamba, D. Borchman, S.K. Sinha, S. Lal, M.C. Yappert, M.F. Lou, Structure and molecular conformation of anhydrous and of aqueous sphingomyelin bilayers determined by infrared and Raman spectroscopy, J. Mol. Struct. 248 (1991) 1–24.
[23] Y. Barenholz, J. Suurkuusk, D. Mountcastle, T.E. Thompson, R.L. Biltonen, A calorimetric study of thermotropic behavior of aqueous dispersions of natural and synthetic sphingomyelins, Biochemistry 15 (1976) 2441–2447.
[24] D.A. Mannock, T.J. McIntosh, X. Jiang, D.F. Covey, R.N. McElhaney, Effects of natural and enantiomeric cholesterol on the thermotropic phase behavior and structure of egg sphingomyelin bilayer membranes, Biophys. J. 84 (2003) 1038–1046.
[25] J. Umemura, D.G. Cameron, H.H. Mantsch, A Fourier transform infrared spectroscopic study of the molecular interaction of cholesterol with 1,2-dipalmitoyl-*sn*-glycero-3-phosphocholine, Biochim. Biophys. Acta 602 (1980) 32–44.
[26] M.B. Sankaram, T.E. Thompson, Interaction of cholesterol with various glycerophospholipids and sphingomyelin, Biochemistry 29 (1990) 10670–10675.
[27] T.N. Estep, D.B. Mountcastle, Y. Barenholz, R.L. Biltonen, T.E. Thompson, Thermal behavior of synthetic sphingomyelin–cholesterol dispersions, Biochemistry 18 (1979) 2112–2117.
[28] T.K.M. Nyholm, M. Nylund, J.P. Slotte, A calorimetric study of binary mixtures of dihydrosphingomyelin and sterols, sphingomyelin, or phosphatidylcholine, Biophys. J. 84 (2003) 3138–3146.
[29] P.R. Maulik, G.G. Shipley, *N*-palmitoyl sphingomyelin bilayers: structure and interactions with cholesterol and dipalmitoylphosphatidylcholine, Biochemistry 35 (1996) 8025–8034.
[30] R.F.M. de Almeida, A. Fedorov, M. Prieto, Sphingomyelin/phosphatidylcholine/cholesterol phase diagram: boundaries and composition of lipid rafts, Biophys. J. 85 (2003) 2406–2416.
[31] A. Filippov, G. Oradd, G. Lindblom, The effect of cholesterol on the lateral diffusion of phospholipids in oriented bilayers, Biophys. J. 84 (2003) 3079–3086.
[32] C. Chachaty, D. Rainteau, C. Tessier, P.J. Quinn, C. Wolf, Building up of the liquid-ordered phase formed by sphingomyelin and cholesterol, Biophys. J. 88 (2005) 4032–4044.
[33] M.I. Collado, F.M. Goni, A. Alonso, D. Marsh, Domain formation in sphingomyelin/cholesterol mixed membranes studied by spin-label electron spin resonance spectroscopy, Biochemistry 44 (2005) 4911–4918.
[34] W. Hübner, A. Blume, Interactions at the lipid–water interface, Chem. Phys. Lipids 96 (1998) 99–123.
[35] M. Rujoi, D. Borchman, D.B. DuPre, M.C. Yappert, Interactions of Ca^{2+} with sphingomyelin and dihydrosphingomyelin, Biophys. J. 82 (2002) 3096–3104.
[36] D.J. Moore, M.E. Rerek, R. Mendelsohn, FTIR spectroscopy studies of the conformational order and phase behavior of ceramides, J. Phys. Chem. B 10 (1997) 8933–8940.
[37] H. Torii, T. Tatsumi, T. Kanazawa, M. Tasumi, Effects of intermolecular hydrogen-bonding interactions on the amide I mode of *N*-methylacetamide: matrix-isolation infrared studies and ab initio molecular orbital calculations, J. Phys. Chem. B 102 (1998) 309–314.
[38] H. Torii, T. Tatsumi, M. Tasumi, Effects of hydration on the structure, vibrational wavenumbers, vibrational force field and resonance Raman intensities of *N*-methylacetamide, Journal of Raman Spectroscopy 29 (1998) 537–546.
[39] L. Ter-Minassian-Saraga, E. Okamura, J. Umemura, T. Takenaka, Fourier transform infrared-attenuated total reflection spectroscopy of hydration of dimyristoylphosphatidylcholine multibilayers, Biochim. Biophys. Acta 946 (1988) 417–423.
[40] E. Mombelli, R. Morris, W. Taylor, F. Fraternali, Hydrogen-bonding propensities of sphingomyelin in solution and in a bilayer assembly: a molecular dynamics study, Biophys. J. 84 (2003) 1507–1517.
[41] S.W. Chiu, S. Vasudevan, E. Jakobsson, R.J. Mashl, H.L. Scott, Structure of sphingomyelin bilayers: a simulation study, Biophys. J. 85 (2003) 3624–3635.
[42] G.A. Khelashvili, H.L. Scott, Combined Monte Carlo and molecular dynamics simulation of hydrated 18:0 sphingomyelin–cholesterol lipid bilayers, J. Chem. Phys. 120 (2004) 9841–9847.
[43] P. Niemela, M.T. Hyvonen, I. Vattulainen, Structure and dynamics of sphingomyelin bilayer: insight gained through systematic comparison to phosphatidylcholine, Biophys. J. 87 (2004) 2976–2989.
[44] E. Mueller, A. Giehl, G. Schwarzmann, K. Sandhoff, A. Blume, Oriented 1,2-dimyristoyl-*sn*-glycero-3-phosphorylcholine/ganglioside membranes: a Fourier transform infrared attenuated total reflection spectroscopic study. Band assignments; orientational, hydrational, and phase behavior; and effects of Ca^{2+} binding, Biophys. J. 71 (1996) 1400–1421.
[45] B. Steinbauer, T. Mehnert, K. Beyer, Hydration and lateral organization in phospholipid bilayers containing sphingomyelin: a ^{2}H-NMR study, Biophys. J. 85 (2003) 1013–1024.
[46] T. Rog, M. Pasenkiewicz-Gierula, Cholesterol–sphingomyelin interactions: a molecular dynamics simulation study, Biophys. J. 91 (2006) 3756–3767.
[47] M. Jackson, D.S. Johnston, D. Chapman, Differential scanning calorimetric and Fourier transform infrared spectroscopic investigations of cerebroside polymorphism, Biochim. Biophys. Acta 944 (1988) 497–506.